Absorption Cross Section Measurement of a Vehicle in Reverberation Chamber for Quick Estimation of Field Strength

Qian Xu, *Member, IEEE*, Xueqi Shen, Kai Chen, Yongjiu Zhao and Yi Huang, *Senior Member, IEEE*

***Abstract*—The average absorption cross section (ACS) of a car in the frequency range of 80 MHz – 24 GHz is measured in a reverberation chamber (RC) based on the time domain method. The measured ACS of a car is very useful: it can be used to predict the electric field strength in a given RC loaded with a car, which can accelerate the calibration process of the RC greatly. The measurement results are provided with uncertainties. Summary on potential applications is also given.**

***Index Terms*—Absorption cross section, reverberation chamber.**

I. Introduction

THE absorption cross section (ACS) of an object is defined as the ratio of the power dissipated in the object to the power density of the incident plane wave. Reverberation chambers (RCs) have been widely used in the ACS measurement [1-10], and the measured ACS is an averaged value over all incident angles.

Generally, two methods have been proposed in the ACS measurement: the frequency domain (FD) method and the time domain (TD) method. Theoretically, these two methods are equivalent; however, the TD method converges faster than the FD method because the chamber decay time (or Q factor) measured in the TD converges faster than that in the FD [11]. Thus, for the same number of samples, the ACS measured in the TD has lower uncertainties than that measured in the FD [11, 12]. Another advantage for the TD method is that the insertion loss from the cables and the antennas will not affect the measurement results, but the loss from the diffused waves determines the chamber decay time.

The ACSs of a human body [4, 7, 9], absorption materials [5], and printed circuit board [8] have been measured. Although RCs have been widely used in electromagnetic compatibility (EMC) measurements for vehicles for years, the ACS of a car has not been quantified. In vehicle EMC test, an RC loaded with a car needs to be calibrated to know how much input power is enough to achieve the required field strength in the EMC test [13]. This measurement is normally performed in the FD using a signal generator, a power amplifier and a field probe. However, this measurement process is relatively time consuming: we need to set the working frequency of the field probe (to have a correct calibration factor), record the E-field values for all the frequencies of interest and stirrer positions. Although this measurement can be performed faster using a vector network analyzer (VNA), inherently, the FD measurement converges slower than the TD measurement [11], thus the statistical variation in the FD measurement is larger than that in the TD measurement. The insertion loss of cables and antennas needs to be removed in the FD measurement but they do not affect the results in the TD measurement.

In this paper, we measure the average ACS of a car in the frequency range of 80 MHz – 24 GHz. In EMC measurements, it is often necessary to estimate the electric field strength in an RC loaded with a car before the RC is constructed. Once the typical ACS of a car is known, we only need to measure the Q factor of an unloaded RC, and the Q factor of the RC loaded with a car can be predicted (without loading a real car). This is

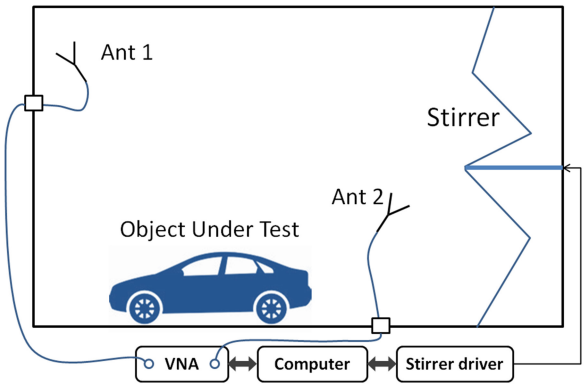

(a)

(b)

Fig. 1. Measurement setup, (a) schematic plot, (b) measurement scenario, an exhaust pipe is also included.

Manuscript received February 2019. This work was supported in part by the National Natural Science Foundation of China under Grants 61701224, and in part by Nanjing Rongce Testing Technology Ltd.

Q. Xu and Y. Zhao are with College of Electronic and Information Engineering, Nanjing University of Aeronautics and Astronautics, Nanjing 211106, China (e-mail: emxu@foxmail.com; yjzhao@nuaa.edu.cn).

X. Shen and K. Chen are with Nanjing Rongce Testing Technology Ltd, Nanjing, 211112, China (e-mail: george@emcdir.com).

Y. Huang is with the Department of Electrical Engineering and Electronics, University of Liverpool, Liverpool L69 3GJ, U.K. (e-mail: yi.huang@liverpool.ac.uk)

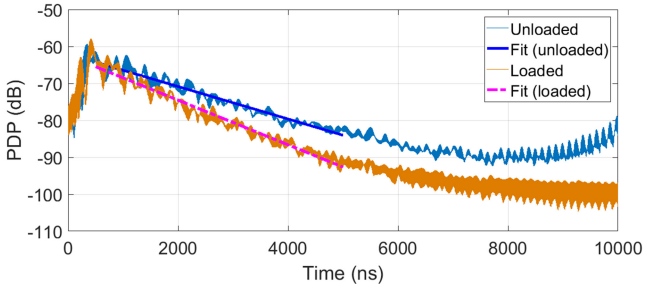

(a)

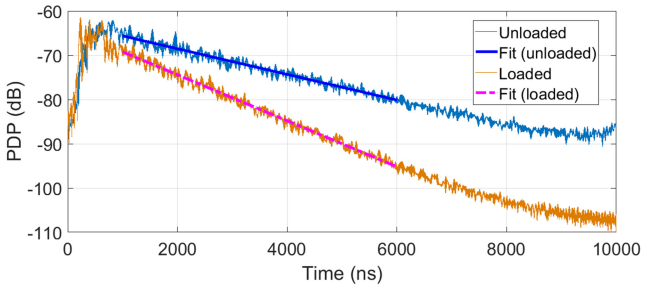

(b)

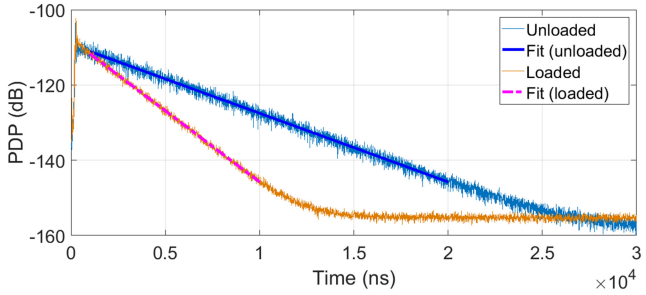

(c)

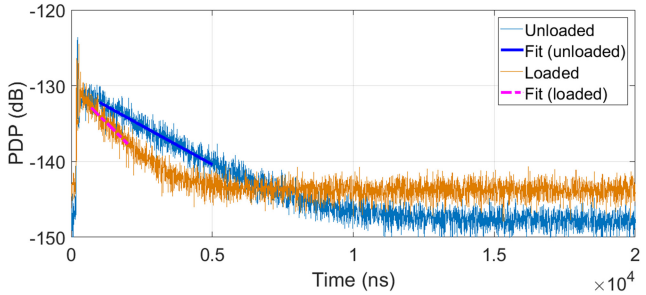

(d)

Fig. 2. Measured PDP of the loaded and unloaded RC, the center frequencies are (a) 80 MHz, (b) 200 MHz, (c) 10 GHz and (d) 24 GHz.

very useful before the RC is constructed, as once the RC is built the unloaded Q factor cannot be increased.

The measurement methodology and the configurations are presented in Section II, Section III details the measurement results and uncertainty analysis, and Section IV summarizes the paper.

II. Theory and Measurement Setup

The average ACS of an object under test can be measured using [11, 14, 15]

$$\langle \mathrm{ACS} \rangle = \frac{V}{c_0}\left(\frac{1}{\langle \tau_l \rangle} - \frac{1}{\langle \tau_u \rangle}\right) \tag{1}$$

where V is the volume of the RC, $c_0 = 3 \times 10^8\ m/s$ is the speed of light in free space, $\langle \tau_l \rangle$ is the decay constant of the loaded RC averaged over all measured stirrer positions, $\langle \tau_u \rangle$ is the averaged decay constant of the unloaded RC, and $\langle \cdot \rangle$ means the average operation over all stirrer positions.

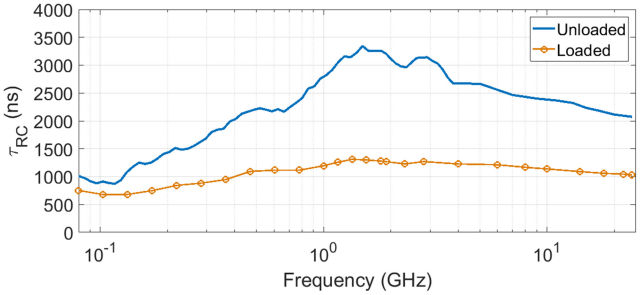

Fig. 3. Measured chamber decay constant of the loaded and unloaded RC.

The schematic plot of the measurement setup in an RC is illustrated in Fig. 1(a), Ant 1 and Ant 2 are broadband antennas which are connected to port 1 and port 2 of the VNA respectively. Log-periodic antennas (or biconical antennas) are used for frequencies lower than 1 GHz, while horn antennas are used for frequencies higher than 1 GHz. A computer synchronizes the frequency sweeping of the VNA and the moving of the stirrer, i.e. for each stirrer position, the computer controls the trigger of the VNA and records the measured *S*-parameters. The measurement scenario is shown in Fig. 1(b), where the RC is loaded with a car. The inner dimensions of the RC are 10.8 m × 12.6 m × 6 m, and the lowest usable frequency [16] is lower than 80 MHz. The stirrer is an oscillating wall which is controlled by a computer to stir the field inside the RC.

III. Measurement Results

To obtain the chamber decay constant $\langle \tau_l \rangle$ and $\langle \tau_u \rangle$, we measure the FD response (S_{21}) and apply the inverse Fourier transform (IFT) to obtain the TD response [11, 12]

$$s_{21}(t) = \mathrm{IFT}\left[\tilde{S}_{21}(f)\right] \tag{2}$$

where $\tilde{S}_{21}(f)$ means the filtered *S*-parameters [17] for a given center frequency (the frequency of interest). The power delay profile (PDP) can be obtained from the average of received power for all stirrer positions:

$$\mathrm{PDP}(t) = \langle s_{21}^2(t) \rangle \tag{3}$$

From the PDP, the chamber decay constant can be extracted by using the least squares method [12], because the PDP decays exponentially when the waves in the RC are well diffused. The decay speed is determined by the chamber decay constant τ_{RC} [11, 12, 14, 15]

$$\mathrm{PDP}(t) \sim P_0 e^{-t/\tau_{RC}} \tag{4}$$

By fitting the slope (k) of the PDP in log scale, τ_{RC} can be obtained as [11, 12, 14, 15]

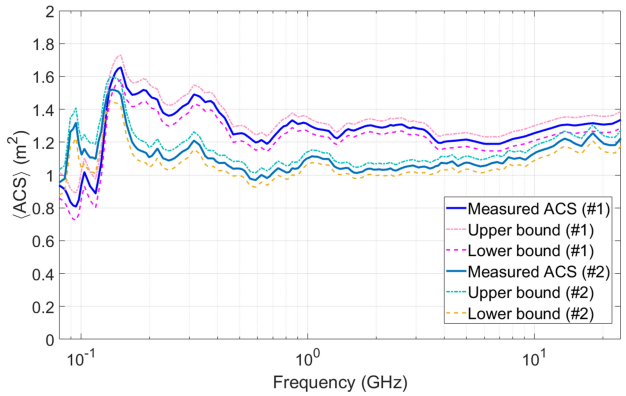

Fig. 4. Measured average ACS and error bounds of a car.

$$\tau_{RC} = -\frac{10}{kln10} \tag{5}$$

For the IFT process in this paper, a relative bandwidth of 10% is used for the center frequencies lower than 1 GHz, and 200 MHz bandwidth is used for frequencies higher than 1 GHz. To have a good TD resolution, the frequency sampling interval of the VNA is set to be smaller than the coherence bandwidth of the unloaded RC [12]. The measured PDPs for different center frequencies are given in Fig. 2(a)-(d), the early-time response and the late-time noise level are avoided in the least squares fitting. Note that when the frequency is high (24 GHz), the cable loss is significant and the noise level is increased, but we still have at least 10 dB signal-to-noise ratio. To measure the PDP at even higher frequencies, an amplifier is required to increase the dynamic range of S_{21}.

By repeating the least squares fitting process for different center frequencies and sweeping center frequency from 80 MHz to 24 GHz, the chamber decay constant for the loaded ($\langle\tau_l\rangle$) and unloaded ($\langle\tau_u\rangle$) RC can be obtained as in Fig. 3.

Considering the uncertainty of τ_{RC} in the loaded and unloaded RC, the error bound for one stirrer position is about $\pm 10\%$ [11]. In this paper, we used 36 stirrer positions, thus the error bound for $\langle\tau_l\rangle$ and $\langle\tau_u\rangle$ can be estimated as $\pm 10\%/\sqrt{36} \approx \pm 1.7\%$. The error propagation in (1) can be derived as [18]

$$\sigma_{\langle ACS\rangle} = \frac{V}{c_0}\sqrt{\frac{\sigma^2_{\langle\tau_l\rangle}}{\langle\tau_l\rangle^4} + \frac{\sigma^2_{\langle u\rangle}}{\langle\tau_u\rangle^4}} \approx \frac{V}{c_0}\sqrt{\frac{1}{\langle\tau_l\rangle^2} + \frac{1}{\langle\tau_u\rangle^2}} \times 1.7\% \tag{6}$$

where σ_* is the uncertainty of '*' (absolute value). From (1) and (6), the measured average ACS and the error bound are presented in Fig. 4 with #1, the relative error bound of the measured ACS is in $\pm 10.4\%$. We have also repeated the measurement with another car with similar size; the results are illustrated in Fig. 4 with #2. It is interesting to note that the ACS differences of #1 and #2 are not large and the loading effects are similar.

IV. Summary

The average ACS of a car has been measured in the RC using the TD method. The ACS for different cars may vary, but a typical value is required. The measurement uncertainties (error bounds) have also been estimated which is very small ($\pm 10.4\%$). From the measured ACS we can estimate the electric-field (E-field) strength for a given input power without actually load the RC with a car. We can also use radio absorbing materials with the same ACS to emulate the loading effect. Suppose an unloaded RC has a decay constant of $\langle\tau_u\rangle$, the mean value of the magnitude of the E-field rectangular components can be obtained as [14-16, 19]

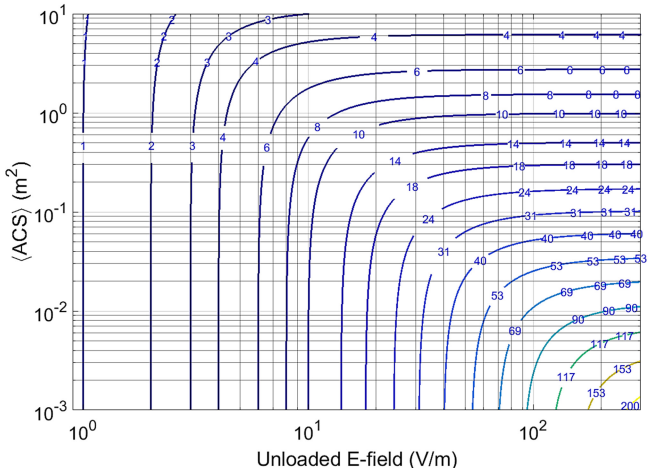

Fig. 5. The contour plot of (8), the x-axis is $\langle|E_x|\rangle_u$ and the contour lines represent $\langle|E_x|\rangle_l$ in (8).

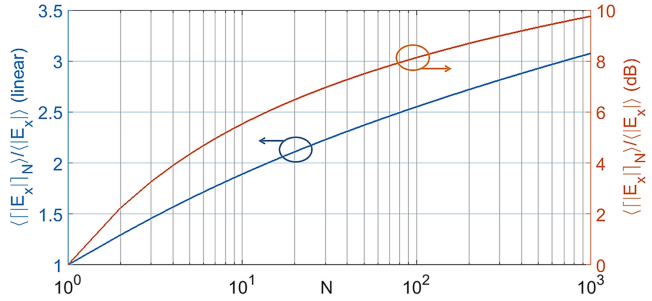

Fig. 6. The ratio of the mean maximum value and the mean value, dB values are also given.

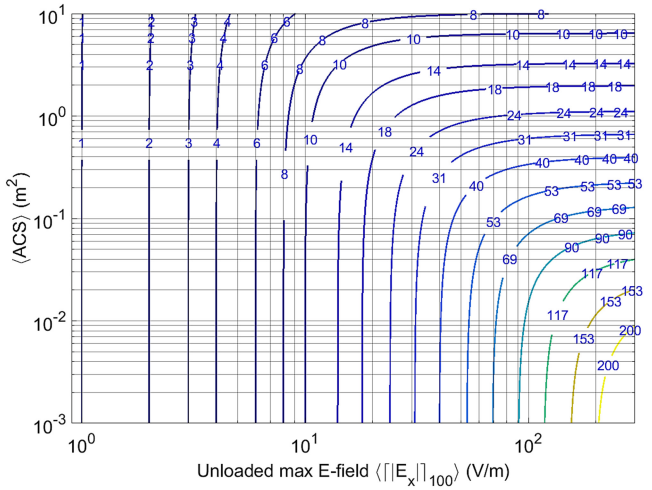

Fig. 7. The contour plot of $\langle\lceil|E_x|\rceil_{100}\rangle$, the x-axis is the value in an unloaded RC, the contour lines are the corresponding values in a loaded RC.

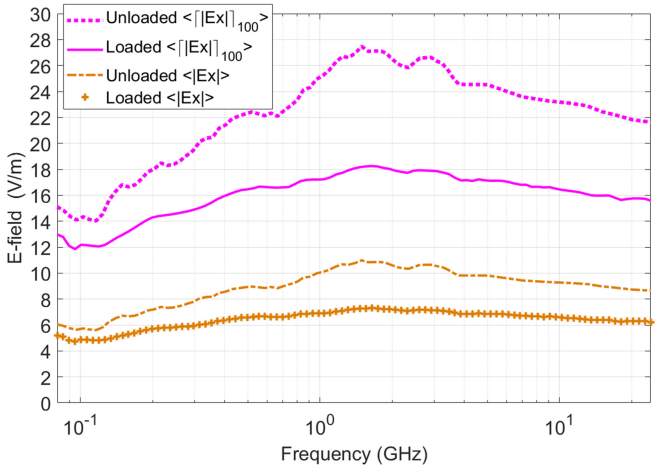

Fig. 8. Estimated normalized E-fields (1W power input), the expectations of the maximum E-fields (loaded and unloaded) with 100 independent sample number and the mean values are given. The ACS of vehicle #1 is used to calculate the loaded E-fields.

$$\langle |E_x| \rangle_u = \sqrt{\frac{5\pi Q \lambda P_{in}}{V}} = \pi \sqrt{\frac{10 c_0 \langle \tau_u \rangle P_{in}}{V}} \tag{7}$$

where $\langle |E_x| \rangle_u$ can be $\langle |E_y| \rangle_u$ or $\langle |E_z| \rangle_u$ which represents the mean value of the magnitude of the rectangular E-field component, the subscript 'u' represents the unloaded RC, P_{in} is the net input power (excluding the insertion loss), Q is the chamber Q factor, and λ is the wavelength. From (1) and (7), the E-field (for 1 W input power) for the RC loaded with a car can be derived as

$$\langle |E_x| \rangle_l = \frac{\pi \sqrt{10}}{\sqrt{\langle \mathrm{ACS} \rangle + 10\pi^2 / \langle |E_x| \rangle_u^2}} \tag{8}$$

A contour plot is illustrated in Fig. 5. Normally the maximum E-field is used for EMC applications. For an independent sample number of N, the maximum E-field has a probability density function (PDF) of [15, 19]

$$\mathrm{PDF}(\lceil |E_x| \rceil_N) = \frac{Nx}{\sigma^2} \left[1 - \exp\left(\frac{-x^2}{2\sigma^2} \right) \right]^{N-1} \exp\left(\frac{-x^2}{2\sigma^2} \right) \tag{9}$$

where $x = \lceil |E_x| \rceil_N = \max(|E_{x1}|, |E_{x2}|, \ldots, |E_{xN}|)$ is the peak value of N independent samples, $\sigma\sqrt{\pi/2}$ is the mean value of $|E_x|$. The ratio of $\langle \lceil |E_x| \rceil_N \rangle$ and $\langle |E_x| \rangle$ can be obtained as [15, 19]

$$\frac{\langle \lceil |E_x| \rceil_N \rangle}{\langle |E_x| \rangle} = \frac{\int_0^\infty N x^2 \left[1 - \exp\left(\frac{-x^2}{2} \right) \right]^{N-1} \exp\left(\frac{-x^2}{2} \right) dx}{\sqrt{\pi/2}} \tag{10}$$

which is evaluated numerically in Fig. 6, thus the maximum E-field can also be evaluated using (8) after converting $\langle \lceil |E_x| \rceil_N \rangle$ to $\langle |E_x| \rangle$. When $N = 100$, the contour plot is illustrated in Fig. 7. From the unloaded decay constant $\langle \tau_u \rangle$ or Q factor, by applying (7), (8) and (10), the estimated E-fields (including the maximum and the mean values) can be obtained and are illustrated in Fig. 8. Although a car has been used in this paper, the method is general and suitable for other equipment/devices under test.

REFERENCES

[1] U. Carlberg, P. -S. Kildal, A. Wolfgang, O. Sotoudeh and C. Orlenius, "Calculated and measured absorption cross sections of lossy objects in reverberation chamber," *IEEE Transactions on Electromagnetic Compatibility*, vol. 46, no. 2, pp. 146-154, May 2004.

[2] A. Gifuni, A. Sorrentino, G. Ferrara, M. Migliaccio, A. Fanti and G. Mazzarella, "Measurements on the reflectivity of materials in a Reverberating Chamber," *Loughborough Antennas & Propagation Conference*, Loughborough, 2011, pp. 1-4.

[3] Z. Tian, Y. Huang, Q. Xu, T. Loh and C. Li, "Measurement of absorption cross section of a lossy object in reverberation chamber without the need for calibration," *Loughborough Antennas & Propagation Conference (LAPC)*, Loughborough, 2016, pp. 1-5.

[4] G. C. R. Melia, M. P. Robinson, I. D. Flintoft, A. C. Marvin and J. F. Dawson, "Broadband measurement of absorption cross section of the human body in a reverberation chamber," *IEEE Transactions on Electromagnetic Compatibility*, vol. 55, no. 6, pp. 1043-1050, Dec. 2013.

[5] G. Gradoni, D. Micheli, F. Moglie, and V. Mariani Primiani, "Absorbing cross section in reverberation chamber: experimental and numerical results," *Progress in Electromagnetics Research B*, vol. 45, pp. 187-202, 2012.

[6] I. D. Flintoft, S. J. Bale, S. L. Parker, A. C. Marvin, J. F. Dawson and M. P. Robinson, "On the measurable range of absorption cross section in a reverberation chamber," *IEEE Transactions on Electromagnetic Compatibility*, vol. 58, no. 1, pp. 22-29, Feb. 2016.

[7] A. Bamba, D. P. Gaillot, E. Tanghe, G. Vermeeren, W. Joseph, M. Lienard, and L. Martens, "Assessing whole-body absorption cross section for diffuse exposure from reverberation chamber measurements," *IEEE Transactions on Electromagnetic Compatibility*, vol. 57, no. 1, pp. 27-34, Feb. 2015.

[8] S. L. Parker, I. D. Flintoft, A. C. Marvin, J. F. Dawson, S. J. Bale, M. P. Robinson, M. Ye, C. Wan and M. Zhang, "Absorption cross section measurement of stacked PCBs in a reverberation chamber," *Asia-Pacific International Symposium on Electromagnetic Compatibility (APEMC)*, Shenzhen, 2016, pp. 991-993.

[9] X. Zhang, M. Robinson, I. Flintoft, J. Dawson, and S. Parker, "Morphological study on human body absorption cross section in a reverberation chamber from 1 GHz to 16 GHz," *IEEE Transactions on Electromagnetic Compatibility*, accepted, 2019.

[10] Q. Xu, Y. Huang, L. Xing, Z. Tian, J. Zhou, A. Chen, and Y. Zhuang, "Average absorption coefficient measurement of arbitrarily shaped electrically large objects in a reverberation chamber," *IEEE Transactions on Electromagnetic Compatibility*, vol. 58, no. 6, pp. 1776-1779, Dec. 2016.

[11] Z. Tian, *Efficient Measurement Techniques in Reverberation Chamber*, PhD thesis, Electrical Engineering and Electronics, University of Liverpool, 2017.

[12] Q. Xu, Y. Huang, L. Xing and Z. Tian, "Extract the decay constant of a reverberation chamber without satisfying Nyquist criterion," *IEEE Microwave and Wireless Components Letters*, vol. 26, no. 3, pp. 153-155, Mar. 2016.

[13] SAE International, *Surface Vehicle Recommended Practice, J551-16*, Oct. 2017.

[14] D. A. Hill, *Electromagnetic Fields in Cavities: Deterministic and Statistical Theories*, Hoboken, NJ, USA: Wiley, 2009.

[15] Q. Xu and Y. Huang, *Anechoic and Reverberation Chambers: Theory, Design and Measurements*, Wiley-IEEE, 2019.

[16] *Electromagnetic Compatibility (EMC)—Part 4-21: Testing and Measurement Techniques—Reverberation Chamber Test Methods*, IEC Standard, IEC 61000-4-21, 2011.

[17] Q. Xu, Y. Huang, Y. Zhao, L. Xing, Z. Tian and T. H. Loh, "Investigation of bandpass filters in the time domain signal analysis of reverberation chamber," *XXXII General Assembly and Scientific Symposium of the International Union of Radio Science (URSI GASS)*, Montreal, QC, 2017, pp. 1-4.

[18] S. Bell, *The Beginner's Guide to Uncertainty of Measurement*, National Physical Laboratory, Mar. 2001.
[19] J. Ladbury, G. Koepke and D. Camell, *Evaluation of the NASA Langley Research Center Mode-Stirred Chamber Facility*, NIST Technical Note, 1508, Jan. 1999.